dc and ac magnetic properties of thin-walled superconducting niobium cylinders

M. I. Tsindlekht,[1] V. M. Genkin,[1] I. Felner,[1] F. Zeides,[1] N. Katz,[1] Š. Gazi,[2] and Š. Chromik[2]
[1]*The Racah Institute of Physics, The Hebrew University of Jerusalem, 91904 Jerusalem, Israel*
[2]*The Institute of Electrical Engineering SAS, Dúbravská cesta 9, 84104 Bratislava, Slovakia*
(Received 11 May 2014; published 24 July 2014)

We report the results of an experimental study of the dc and ac magnetic properties of superconducting Nb thin-walled cylinders in parallel to the axis magnetic fields. The magnetization curves at various temperatures are measured. Surprisingly, at 4.5 K, for magnetic fields much lower than H_{c1}, avalanchelike jumps of the magnetization are observed. The position of the jumps is not reproducible and changes from one experiment to another, resembling vortex lattice instabilities usually observed for magnetic fields larger than H_{c1}. At temperatures larger than 6.5 K, the measured magnetization curves become smooth. ac response is measured in constant and swept dc magnetic fields. A phenomenological model that describes the ac response of the surface superconducting states is proposed. This model assumes that the observed ac response in dc fields larger than H_{c2} is due to the relaxation of surface superconducting states with nonzero current in the walls to the state with zero current, and the existence of a critical current below which this relaxation is absent.

DOI: 10.1103/PhysRevB.90.014514 PACS number(s): 74.25.F−, 74.25.Op, 74.70.Ad

I. INTRODUCTION

The subject of magnetic field flux in hollow superconducting cylinders has received a great deal of attention from the beginning of modern superconductivity measurements years ago. The Little-Parks effect and quantization of trapped flux were intensively investigated during the last fifty years [1–3]. These effects require small diameters of the cylinders in order to work with a small number of flux quanta in the hollow region. However, thin-walled hollow cylinders with macroscopic diameter have some advantages in research. A large diameter permits to monitor the magnetic moment of the current circulating in the walls and estimate the ac conductivity of the film in the mixed state in swept magnetic fields [4]. Under an axial magnetic field H_0, the cylinder walls screen an external field, if $L \equiv R^2/\lambda d \gg 1$, where R is the cylinder radius, d is the wall thickness, and λ is the London penetration depth [2,5,6]. An external magnetic field can penetrate into the cylinder if the current in the wall begins to exceed its critical value. In the range of dc fields $H_{c1} < H_0 < H_{c2}$, it involves the creation of vortices at the outer surface and subsequent motion inside the cylinder. From this point of view, one can expect that weak magnetic fields below H_{c1} will not penetrate into the cylinder. For $H_0 > H_{c1}$ in a magnetic field perpendicular to Nb films, a surface vortex motion leads to flux jumps [7,8]. These flux jumps were interpreted as thermomagnetic instabilities of the critical state.

Nucleation of the superconducting phase in a thin surface sheath in a decreasing magnetic field parallel to the sample surface was predicted by Saint James and de Gennes [9]. They showed that nucleation of the superconducting phase occurs in a magnetic field $H_0 < H_{c3} \approx 1.695 H_{c2}$. Experimental confirmation of this prediction was carried out a short time after the paper's publication. It was found that low-frequency losses in superconductors in surface superconducting states (SSS) can exceed the losses in a normal state [10,11].

Swept dc magnetic fields considerably changed the character of the ac response. Losses and a penetration ac magnetic field took place not only for $H_{c2} < H_0 < H_{c3}$ but also for $H_{c1} < H_0 < H_{c2}$, where they were not observed in constant dc fields [12–14]. The influence of a swept dc field is more suitably investigated with hollow thin-walled superconducting cylinders because here one can control the transmission of the field through the wall. In Ref. [4], it was shown that for a thin-walled cylinder in the mixed state, the effect of sweeping a dc field on the ac response was due to increasing vortex motion through the wall. Above H_{c2}, this picture is not appropriate whereas the observed ac response does not show any singularity at H_{c2} in thin-walled cylinders. The reason for the lack of singularity in a thin-walled cylinder at H_{c2} is not yet clear. We have to mention that peculiarities of the ac response near H_{c2} in a swept field exist in single crystals Nb [14] and YB_6 [15] as well.

This paper describes dc and ac magnetic properties of superconducting thin-walled Nb cylinders. In the first part, we deal with magnetic flux penetration in magnetic dc fields applied parallel to the cylinder axis. We show that for Nb thin-walled cylinders even at $H_0 < H_{c1}$, the axial (parallel to Nb film) external field penetrates through the cylinder walls in an avalanchelike mode. At 4.5 K, we observed jumps of the magnetic moment not only above H_{c1} but also in fields $H_0 < H_{c1}$. The field at which the first jump occurs, H^*, is changing from one measurement to another. This demonstrates that we are dealing with transitions between metastable states. Above 6.5 K, the jumps disappear and we observe a smooth penetration of dc field into the cylinder. Magnetic flux instabilities in superconducting niobium films in magnetic fields perpendicular to the film surface were studied in Refs. [7,8]. The physical nature of the critical states in our polycrystalline Nb films in the fields below H_{c1} and parallel to the film surface is not yet clear. The second part of the paper is devoted to the study of ac response in a dc field. The signals of the first, second, and third harmonics were measured in constant and swept dc magnetic fields. Experimental results are explained by a proposed phenomenological model of the ac response of the film in the surface superconducting states (SSS). It may be possible to expand this model to also explain the ac response in fields below H_{c2}.

II. EXPERIMENTAL DETAILS

The Nb films were deposited by dc magnetron sputtering at 300 °C (Jerusalem) and room temperatures (Bratislava). Two types of Nb thin film samples have been prepared and measured. The first type, S1, is a planar film deposited on an Si substrate. The second type, S2, is a film deposited on four sides of a sapphire substrate. The sizes of the sapphire substrate with rounded corners (radius 0.2 mm) are $1.5 \times 3 \times 15$ mm^3. We formed, actually, a thin-walled hollow superconducting cylinder with a rectangular cross section. The sapphire substrate was cleaned with ethanol and then installed into a mechanical device that provided double rotation with mutually perpendicular axes: one around the longitudinal substrate axis, and the second, around the upright sputtering machine direction. The device was placed into the sputtering machine chamber, pumped out to the 2×10^{-7} Torr vacuum. A sketch of the cylindrical sample is presented in Fig. 1.

The film structure was characterized by JOEL JSM-7700 scanning electron microscopy (SEM) and two images of S2 films with wall thickness of 100 nm deposited at room temperature (top) and at 300 °C (bottom) are shown in Fig. 2. It is readily seen that the films' morphology is very similar and the experimental results obtained in these two types of samples are qualitatively the same.

dc magnetic properties were measured using a commercial superconducting quantum interference device (SQUID) magnetometer. The ac response was measured by the pick-up coil method. The sample was inserted into one coil of a balanced pair of coils, and the unbalanced signal was measured by a lock-in amplifier. ac magnetic susceptibilities were measured in absolute units, see Ref. [16]. A home-made measurement cell of the experimental setup was adapted to a SQUID magnetometer. The block diagram of the experimental setup has been published elsewhere [16].

Measurements of the ac response as a function of dc field were carried out by two methods. First, the dc field was kept constant during an ac measurement, point-by-point (PBP)

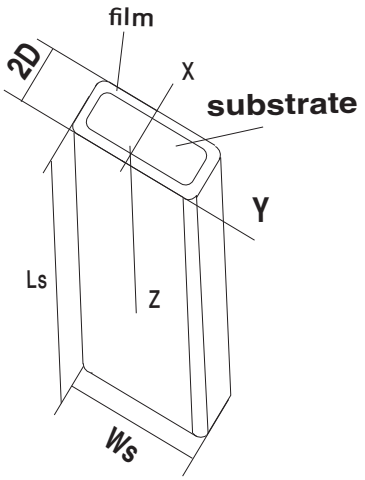

FIG. 1. Sketch of the S2 sample. Here, $L_s = 15$ mm, $W_s = 3$ mm, and $2D = 1.5$ mm are the substrate length, width, and thickness, respectively. Both dc and ac fields were parallel to z axis. Dimensions are not to scale.

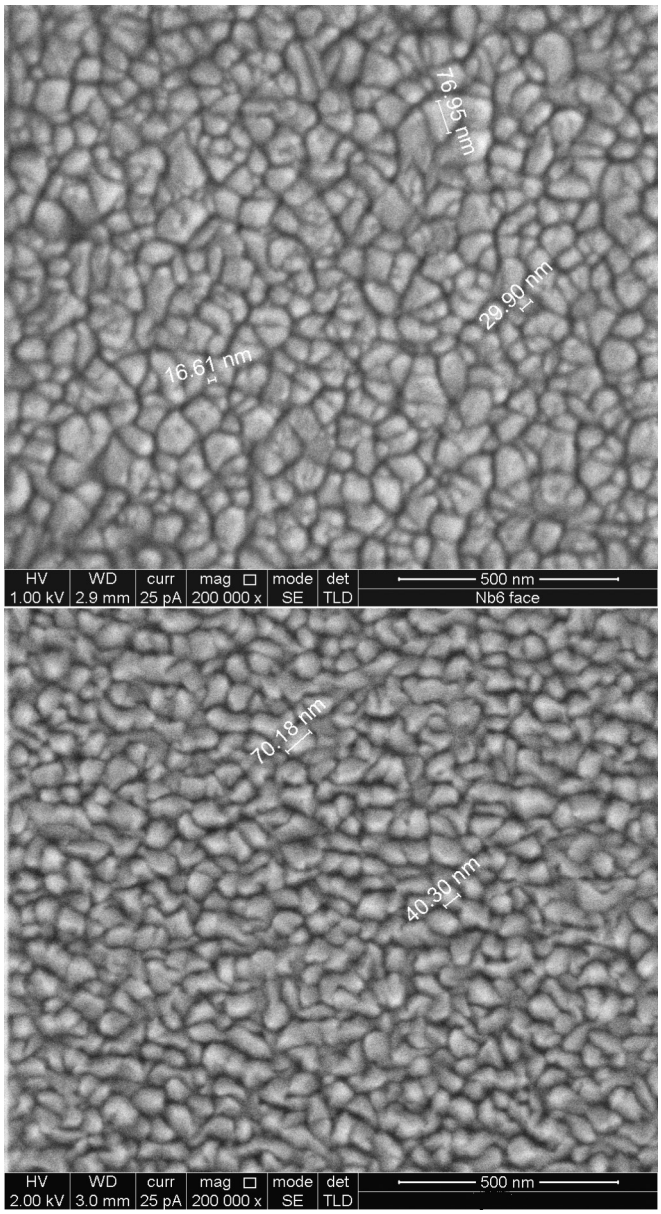

FIG. 2. SEM images of the 100-nm films deposited at room temperature (top) and at 300 °C (bottom).

mode, and in the second method, the dc field was ramped with a given rate, swept field (SF) mode. In the latter case, dc was ramped with rate of 20 Oe/s. For the measurements in a swept field, the power supply of the SQUID magnet was replaced by an external one. Both external ac and dc fields were parallel to the films surface and to the axis of the cylinder. The frequencies were 293 and 1465 Hz, the ac amplitudes 0.04 and 0.2 Oe, and the temperatures were 4.5, 5.5, 6.5, and 7 K.

III. EXPERIMENTAL RESULTS

A. dc magnetization

Magnetic moment temperature and field dependencies of S1 and S2 samples reported here were measured after cooling down to the desired temperatures in a zero-field (ZFC) process.

1. Planar films

A typical magnetic moment M_0 field dependence for the S1 sample (thickness 240 nm) is shown in Fig. 3. At 4.5 K, the estimated $H_{c1} \approx 0.4$ kOe and $H_{c2} \approx 10$ kOe. The Ginsburg-Landau (GL) parameter κ was calculated using formula $H_{c1}/H_{c2} = \ln\kappa/2\kappa$, then $\kappa = 4.2$. Large values of κ for Nb thin films were also reported in Ref. [17]. The upper inset to Fig. 3 shows the temperature dependence of the magnetic moment measured at 20 Oe, from which $T_c \approx 8.9$ K is easily deduced. The temperature dependence of H_{c2} is presented in the lower inset to Fig. 3.

2. Thin-walled cylinders

$M_0(H_0)$ dependence of an S2 sample with wall thickness 300 nm measured at 4.5 and 7 K after ZFC is shown in Fig. 4. The H_{c2} value at 4.5 K (around 10 kOe) is close to that exhibited in Fig. 3 for S1 film. Therefore we assume that the two S1 and S2 samples also have the same H_{c1} value (around 0.4 kOe). Figure 4 shows that magnetization jumps at 4.5 K exist even at $H_0 < H_{c1}$. An expanded view of magnetization curves in low fields is shown in Fig. 5. The field of the first jump H^* is around 30 Oe at 4.5 and 5.5 K and increases to 70 Oe at 6.5 K. At 7 K, this avalanchelike penetration of dc field disappears. This behavior is reminiscent of the magnetic flux jumps in Nb thin films for H_0 perpendicular to the film surface [7,8]. The jumps obtained at $H_0 > H_{c1}$ were interpreted as a thermomagnetic instability of the Abrikosov vortex lattice [7,8]. However, to the best of our knowledge, jumps below H_{c1} have never been observed.

Several minor hysteresis loops of the same S2 cylinder at 4.5 and 6.5 K are shown in Figs. 6(a) and 6(b). The protocol of these measurements is as follows. First, after ZFC to 4.5 K, the field was raised up to $H_0 = 30$ Oe and then decreased to $H_0 = 0$. No hysteresis loop is opened. Next, after heating to a temperature well above T_c, the cylinder was ZFC back to 4.5 K and H_0 was ramped up to 35 Oe and decreased back to zero. Here, a small hysteresis loop is opened. Repeating this procedure, H_0 was ramped further up to 70 Oe. Interestingly, the first jump is obtained at $H_0 = 40$ Oe. In the last cycle, the first jump is at $H_0 = 45$ Oe. This indicates that the jump position is not reproducible and changes from one measurement to another. A similar procedure was applied at 6.5 K [Fig. 6(b)]. Here, H_0 was ramped twice: up to 70 and 80 Oe. In both cases, the jumps are at 60 Oe. Next, H_0 was raised up to 110 Oe and unexpectedly no jumps occurred and a minor hysteresis loop was smoothly opened, indicating once again the instability of this state.

The magnetic field inside the cylinder can be calculated from $H_i = H_0 + 4\pi M_0/V$. In Fig. 7, we showed H_i as a function of applied magnetic field H_0. These data were obtained from a minor hysteresis loop that is shown in the Fig. 6(c). The plateau length in Fig. 7 characterizes the critical current, J_c, value.

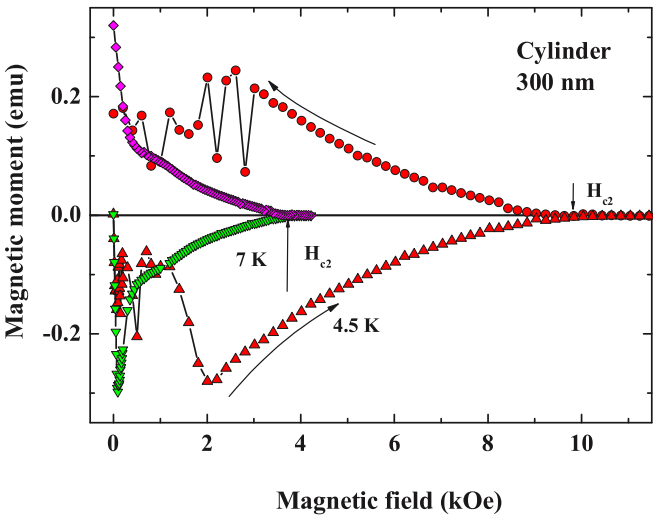

FIG. 4. (Color online) Magnetization curves of S2 sample with thickness 300 nm at 4.5 and 7 K.

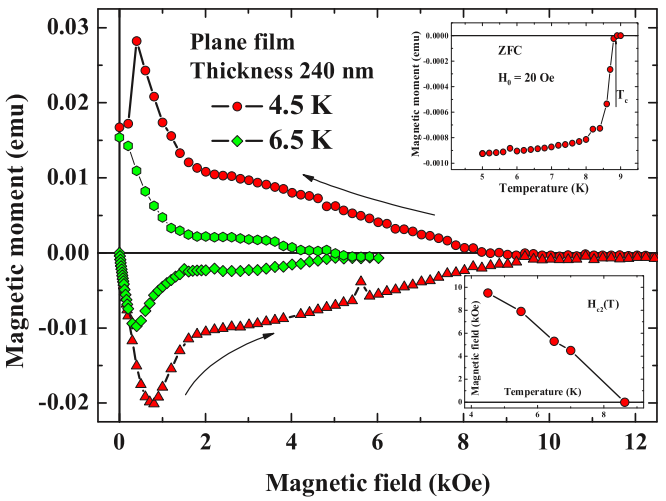

FIG. 3. (Color online) Magnetization curves of the S1 type 240-nm sample at 4.5 and 6.5 K. (Top inset) $M_0(T)$ at $H_0 = 20$ Oe. (Bottom inset) Temperature dependence of H_{c2} for this film.

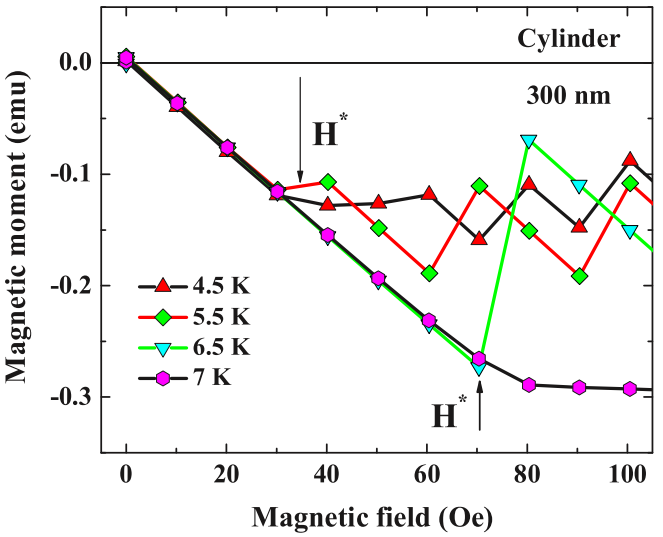

FIG. 5. (Color online) Expanded view of magnetization curves in low magnetic fields.

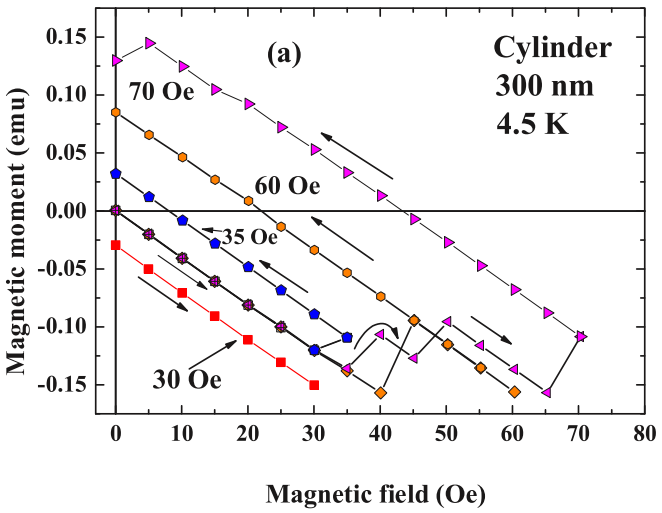

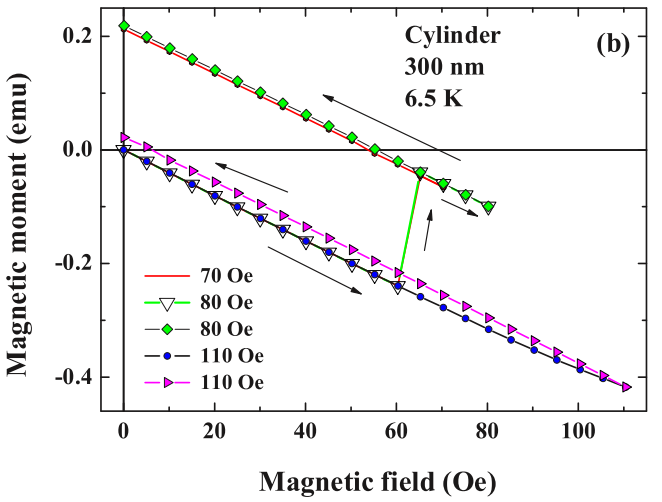

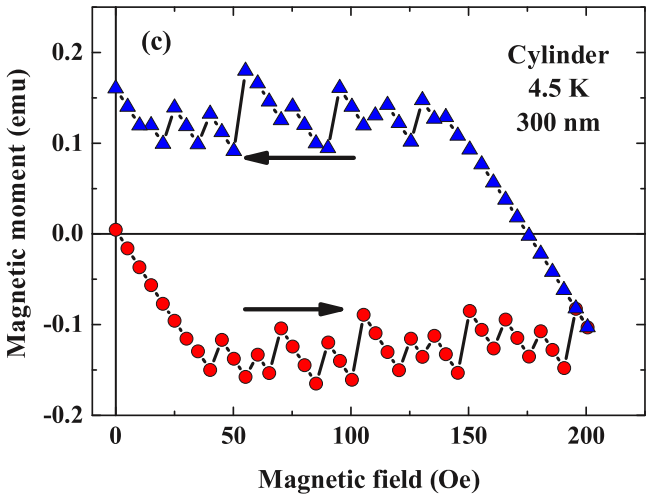

FIG. 6. (Color online) Minor magnetization loops at 4.5 and 6.5 K [(a) and (b), respectively]. The number near the traces designates a maximal field for a given loop. All measurements were done after ZFC. Data for 30 Oe in (a) are shifted for clarity. Minor magnetization loop with maximal $H_0 = 200$ Oe (c). Arrows show the direction changes of the magnetic field. The symbols in legend of (b) indicate maximal field for each loop.

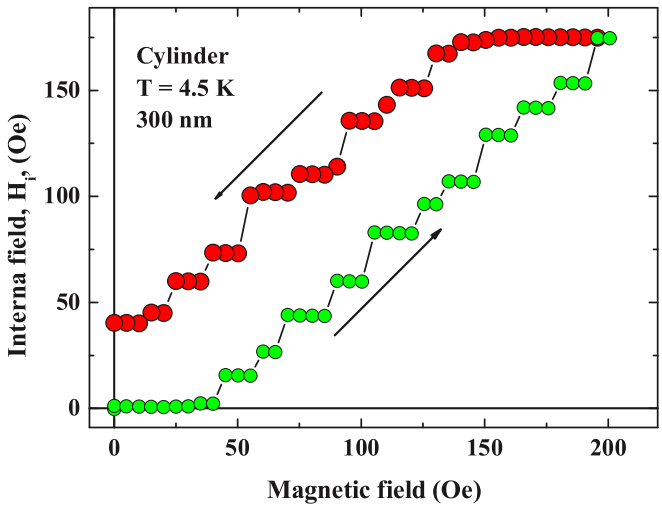

FIG. 7. (Color online) The magnetic field inside the substrate as a function of the applied magnetic field. The plateau length characterizes the value of the critical current, J_c.

Magnetization curves of the S2 cylinder with a film thickness of 60 nm at 4.5, 5.5, and 6.5 K are shown in the upper panel of Fig. 8. Here again, instabilities below H_{c1} are clearly observed at 4.5 K. The normalized to the film thickness $M_0(H_0)$ plots at 4.5 K of the two S2 cylinders 60- and 300-nm thick are shown in Fig. 8 (bottom). It appears that for $H_0 > 3$ kOe, the two curves merge, indicating the same current density at elevated fields. The kink in $M_0(H_0)$ at 4.5 K in $H_0 \approx 2$ kOe, observed also in Figs. 3 and 8, indicates that all films measured are not perfectly uniform.

B. ac response

The technique in which a small axial ac magnetic field with frequency several hundreds of hertz is superimposed upon the coaxial dc field is very fruitful. The effective ac magnetic susceptibility of the sample in the external field,

$$H(t) = H_0(t) + h_{\rm ac}\sin(\omega t), \tag{1}$$

is given by

$$M(t) = V h_{\rm ac}\sum_n [\chi_n' \sin(n\omega t) - \chi_n'' \cos(n\omega t)], \tag{2}$$

and exhibits the appearance of the harmonics of the fundamental frequency, field penetration into cylinder, i.e., $\chi_1' \neq -1/4\pi$, and losses $\chi_1'' > 0$. Here, $M(t)$ is the magnetic moment of the sample and V is its volume. In the following, we consider the results of ac measurements in PBP and SF modes.

1. Point-by-point mode

The real and imaginary ac susceptibility plots at 4.5 K for a cylinder 60-nm thick, measured at various amplitudes and frequencies as a function of H_0 in PBP mode, are shown in Fig. 9. In this mode, a complete screening of the ac field by superconducting walls is observed up to 16.5 kOe, a value which is higher than $H_{c2} = 11$ kOe (Fig. 8). Only near H_{c3}, $H_{c3} \approx 19.2$ kOe, and incomplete shielding, losses, and third harmonic signal are present. The frequency dispersion of χ_1

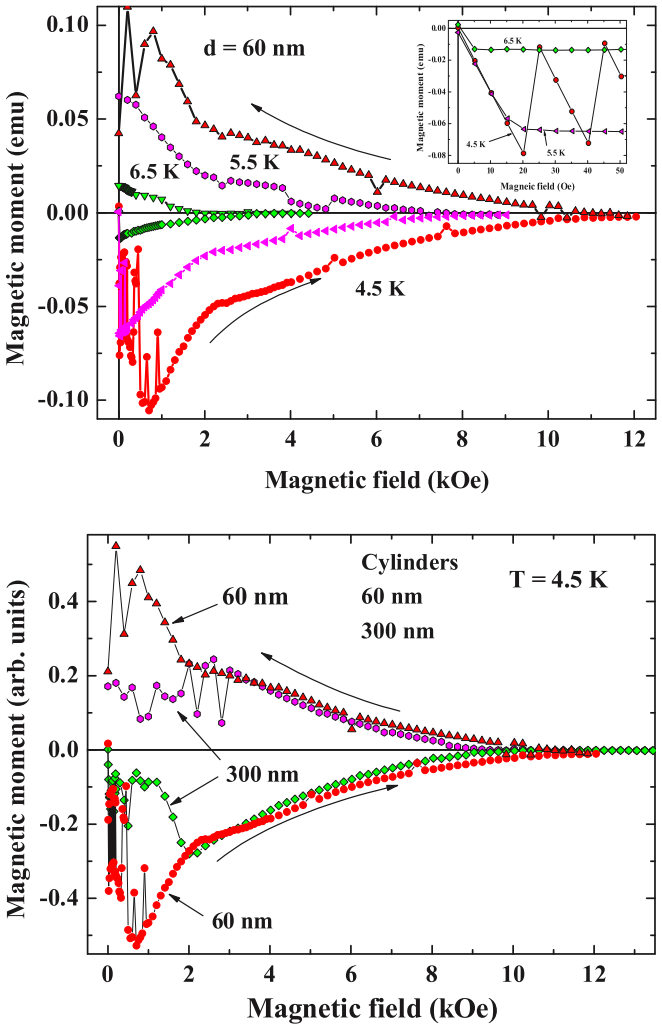

FIG. 8. (Color online) (Top) Magnetic moment of the S2 sample with wall thickness 60 nm as a function of the dc magnetic field at temperatures 4.5, 5.5, and 6.5 K. The inset shows the expanded view of ascending branch $M_0(H_0)$ at low fields. (Bottom) Normalized on the film thickness magnetization curves of two S2 samples with film thicknesses 60 and 300 nm at 4.5 K.

is weak, and the ratio $H_{c3}/H_{c2} \approx 1.75$. Figure 10 shows the field dependence of χ_3 at 4.5 K measured at two frequencies and amplitudes. The third harmonic becomes noticeable near H_{c3}, while the second harmonic is absent.

2. *Swept-field mode*

Figure 11 shows the ac response of the Nb thin-wall cylinder (60-nm-thick) in a swept dc field at the rate 20 Oe/s. In contrast to the PBP mode (Fig. 9), the ac field partially penetrates into the cylinder. Moreover, the losses, the second $|\chi_2|$, and third $|\chi_3|$ harmonics [Fig. 12(a)] are visible even at fields much lower than H_{c2}. In this mode, the frequency dispersion of χ is also observed. Figure 12 shows $|\chi_2|$ and $|\chi_3|$ of a cylinder with 120-nm-thick walls. The solid curves in Figs. 10 and 12 are the theoretical fits proposed by the model described in the next section. We measure that for the SF mode $|\chi_2| > |\chi_3|$.

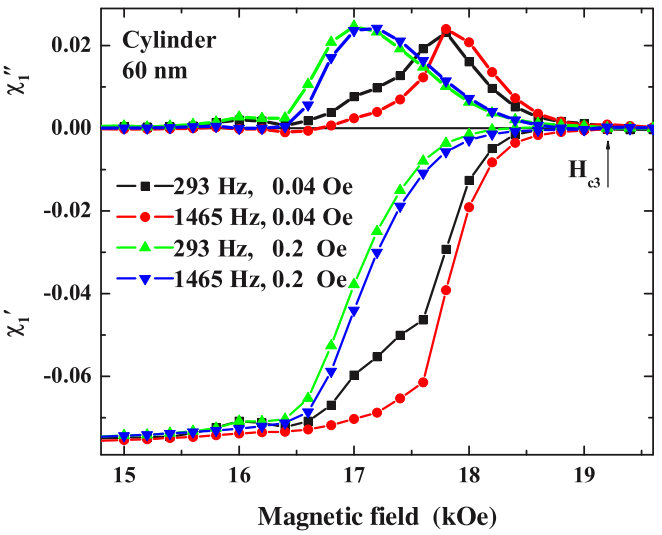

FIG. 9. (Color online) $\chi_1(H_0)$ of S2 sample with film thickness 60 nm at 4.5 K measured in PBP mode.

IV. THEORETICAL BACKGROUND

A. Surface states in the thin-walled hollow cylinder

SSS in the round cylinder are discussed usually in terms of giant vortices [18]. It is assumed that the order parameter in cylindrical coordinates has the form

$$\psi(r,\phi) = \psi_1(r)\exp(im\phi) = \psi_1(r)\exp(i\widetilde{q}l), \qquad (3)$$

where m is an integer number, $\widetilde{q} = m/2\pi r$ and $l = \phi r$ is a line coordinate along the circle with radius r. Our samples have a rectangular cross section with one size larger than the other. We take a model of an infinite slab of thickness $2D$ with a thin superconducting film (thickness d) on both sides, and $d \ll D$. In this case Eq. (3) becomes

$$\psi(x,y) = f(x)\exp(iqy). \qquad (4)$$

Here, the axes are according to those shown in Fig. 1. The magnetic field is along the z axis, and q is as yet undetermined here. It is convenient to introduce dimensionless units: $\psi = \psi_0 f; \widetilde{x} = \lambda(T)x; \frac{2\pi}{\Phi_0}\xi(T)\overrightarrow{A} = \overrightarrow{a}; \frac{2\pi}{\Phi_0}\xi(T)\lambda(T)\overrightarrow{H} = \overrightarrow{h}$, (see p. 30, [19]), here ψ_0 is the order parameter at zero magnetic field, ξ is a correlation length, and $\Phi_0 = hc/2e$ is a flux quantum. Henceforth, we drop the tilde in dimensionless variables, and GL equations in dimensionless variables look as follows:

$$\frac{1}{\kappa^2}\frac{d^2 f}{dx^2} - (a-q)^2 f + f - f^3 = 0,$$
$$\frac{d^2 a}{dx^2} - f^2(a-q) = 0, \qquad (5)$$

where a is the y component of the vector potential, magnetic field $h_z = da/dx$, and current density $j_y = -dh_z/dx$. The dimensionless Gibbs energy is

$$G = [-f^4/2 + (h - h_{\rm ex})^2]dx, \qquad (6)$$

where $h_{\rm ex}$ is the dimensionless external magnetic field. The magnetic field h_i inside the slab is constant, and the vector potential at the inner surface of the wall $a_i = h_i/D$. So, the

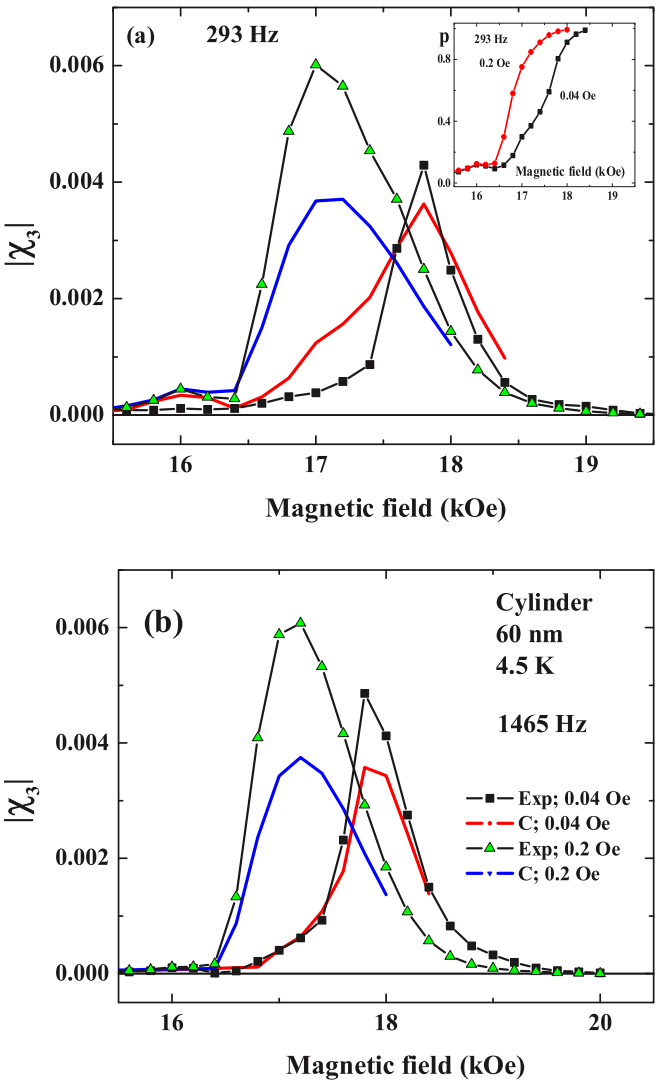

FIG. 10. (Color online) $|\chi_3(H_0)|$ of the cylinder with 60-nm-thick walls at 4.5 K, frequencies 293 and 1465 Hz [(a) and (b), respectively] measured in PBP mode. Lines with "Exp" in the legend correspond to the experimental data, with "Sim" to the simulated data. Inset to (a) shows the part of unpinned SSS as a function of dc fields for two ac amplitudes. The "effective" part of the unpinned SSS increases with ac amplitude (see Discussions).

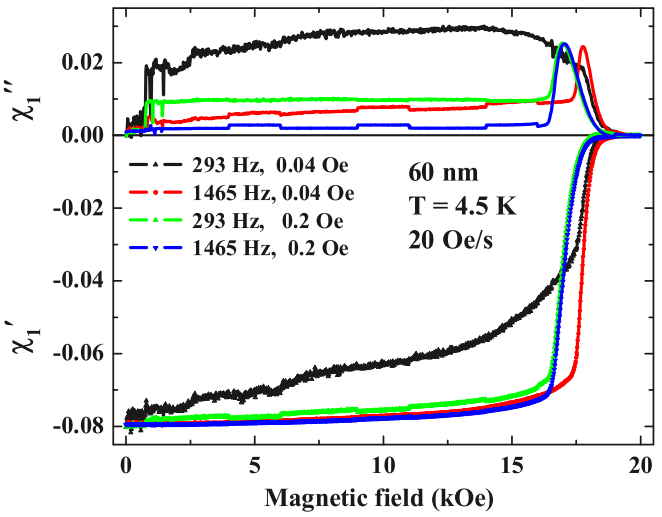

FIG. 11. (Color online) $\chi_1(H_0)$ of the cylinder sample with 60-nm-thick walls at 4.5 K, frequencies 293 and 1465 Hz, ac amplitudes 0.04 and 0.2 Oe, and sweep rate 20 Oe/s.

boundary condition for the vector potential at the inner side of the wall ($x = 0$) is

$$h_i = \frac{da}{dx} = \frac{a_i}{D}, \tag{7}$$

at the outer side ($x = d$)

$$\frac{da}{dx} = h_{\rm ex}. \tag{8}$$

For the wave function, we took the boundary condition $df/dx = 0$ on both sides of the film.

Equations (5) has been investigated analytically and numerically (see, for example, Refs. [2,19]) and we will note here only some features which concern the thin film being the wall of a cylinder. The parameter L (replacing R by D) is $\approx 10^4$ in our case. The total superconducting current in the film J_s is a function of h_0 and q. For a given dc magnetic field, there is a band of allowed q's, and there is $q = q_0(h)$ for which $J_s(h_{\rm ex},q_0) = 0$. In weak magnetic fields, there is also the solution with $q = 0$ and zero magnetic field inside the substrate, Fig. 13 (curve 1). This solution describes the complete shielding of a dc field by the wall. The other solution with $q = q_0$ corresponds to the complete penetration of dc field into the slab. The order parameter for both solutions actually equals to the unperturbed value in zero magnetic field. As the applied magnetic field is increased, the solution with $q = 0$ at some magnetic field vanishes. For type II superconductors, these solutions have physical sense only for magnetic fields below H_{c1}.

For large magnetic fields, SSS could be localized at the internal or external sides of the wall. The properties of these both states are the same. Below H_{c2}, i.e., in the mixed state, SSS could exist too [20]. In Fig. 14, we show the order parameters and magnetic field in the applied field $H_0/H_{c2} = 1.4$ and $q = q_0$ for which the magnetic field completely penetrates into the slab (i.e. $J_s = 0$). Curves 1 (2) correspond to the surface state, which is localized on the inner (outer) side of the wall.

B. Phenomenological model of the ac response of SSS

The current in SSS is a function of the magnetic field and q. Numerical calculations show that in a wide range of magnetic fields below H_{c3}, J_s is a linear function of both arguments and $\partial J_s(h_{\rm ex},q)/\partial h_{\rm ex} = -1$. As a result, for fixed q, SSS can screen the ac field completely. Only in the immediate vicinity of H_{c3} is this violated. For example, for $H/H_{c3} = 0.976$, $\partial J_s(h_{\rm ex},q)/\partial h_{\rm ex} = -0.995$. However, in a wider range of $H_0 < H_{c3}$, incomplete screening by SSS is observed. In a swept dc field, the film is partly transparent for ac field in all H_0 higher than H_{c1}. This shows that q changed during an ac cycle and it is assumed that q relaxes toward the instantaneous value of q_0 for which $J_s(q_0(h_{\rm ex}),h_{\rm ex}) = 0$ [21], i.e.,

$$dq/dt = -\nu[q - q_0(h_{\rm ex})][q - q_0(h_{\rm ex})]. \tag{9}$$

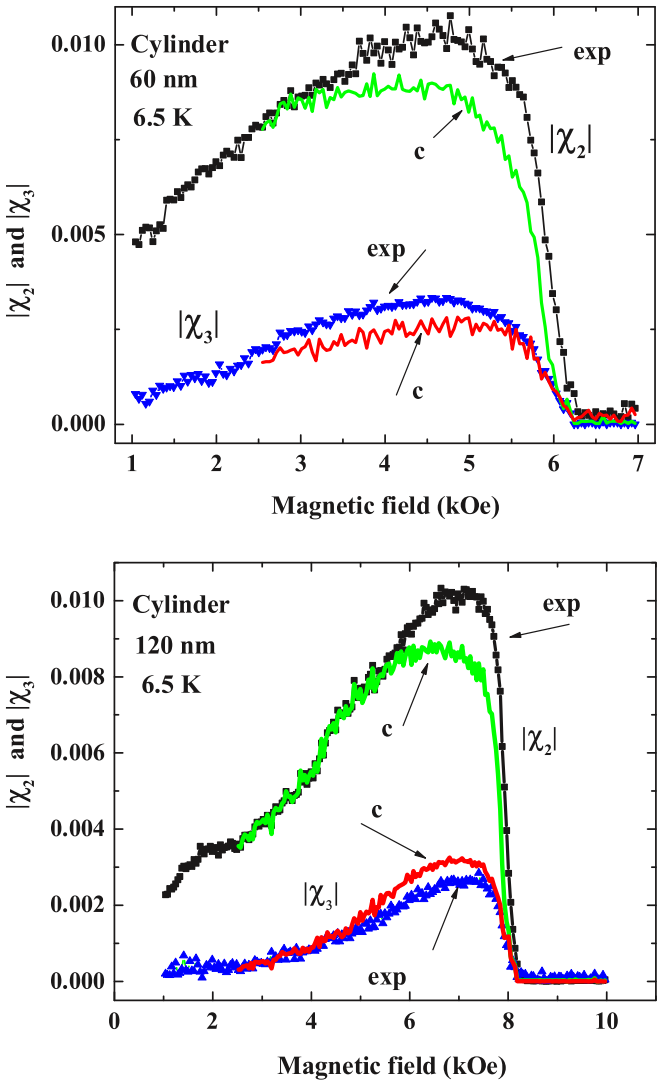

FIG. 12. (Color online) Field dependence of the $|\chi_2|$ and $|\chi_3|$ of the S2 samples with 60-nm (top) and 120-nm (bottom) wall thickness at 6.5 K, frequency 293 Hz, ac amplitude 0.04 Oe, and sweep rate 20 Oe/s. Lines with "exp" correspond to experimental data, with "c" to simulated data (see Discussion).

Introducing a new variable $k = q - q_0(h_{ex})$, we obtain

$$\frac{dk}{dt} = -\nu(k)k - dq_0/dh_{ex} - \frac{dq_0}{dh_{ex}} \times \frac{dh_{ex}}{dt} \qquad (10)$$

and $J_s = k\partial J_s(q,h_{ex})/\partial q$, because J_s is a linear function of k. Multiplying Eq. (9) by $\partial J_s(q,h)/\partial q$, we obtain

$$\frac{dJ_s}{dt} = -\nu(J_s)J_s - \frac{dh_{ex}}{dt}, \qquad (11)$$

where due to $\partial J_s(h_{ex},q)/\partial h_0 = -1$ $(\partial J_s(h_{ex},q_0)/\partial q)(\partial q_0/\partial h_{ex}) = 1$.

The magnetic field inside the substrate is $h_i = J_s + h_{ex}$ (Ampere law). If $\nu(J_s) = 0$ for $|J_s| < J_{pin}$ then Eq. (11) shows that $d(J_s + h_{ex})/dt = 0$ and complete screening of an ac field will be observed. Here, J_{pin} is some "pinning" current of the SSS. An ac field can penetrate through the film if the amplitude of the surface current will exceed J_{pin} and $\nu(J_s) \neq 0$. We assume that in the film there are a lot of SSS' with different J_{pin}

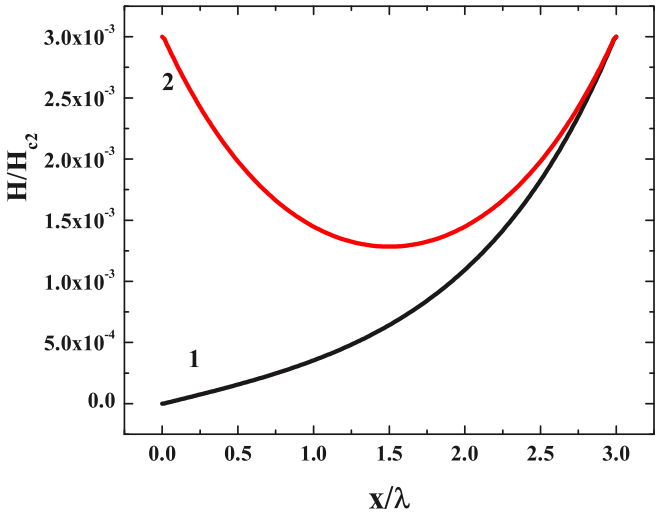

FIG. 13. (Color online) Normalized magnetic field in the wall for shielded (1) and transparent (2) solutions of GL equations. The thickness of the wall $d/\lambda = 3$, $D/d = 5 \times 10^3$, the GL parameter $\kappa = 1.5$, and the applied magnetic field $H_0/H_{c2} = 0.003$. For this set of parameters, the solutions with shielding exist only for $H_0/H_{c2} < 4 \times 10^{-3}$.

and the observed ac response is the combined response of all these states. Further, we simplify this approach by considering only two SSS, one with $J_{pin} = 0$ and another with $J_{pin} \neq 0$. In this approximation, the observed susceptibility can be written as

$$\chi_n = p\chi_{n0} + (1-p)\chi_{np}. \qquad (12)$$

Here, p is a part of unpinned SSS, $0 < p < 1$, and $\chi_{n0}(\chi_{np})$ is the response of the SSS with $J_{pin} = 0$ ($J_{pin} \neq 0$).

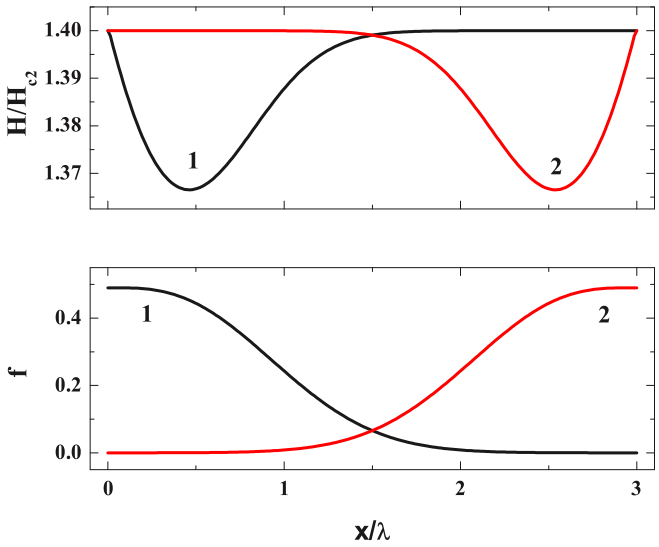

FIG. 14. (Color online) Normalized order parameter and magnetic field for surface states localized at the inner (1) and outer (2) sides of the wall. The total current in these states equals zero. The thickness of the film $d/\lambda = 3$, the Ginzburg-Landau parameter $\kappa = 1.5$, and the applied magnetic field $H_0/H_{c2} = 1.4$.

V. DISCUSSION

A. Magnetization curves

The experimental data demonstrate the existence of magnetic instabilities in fields smaller than H_{c1}. At 4.5 K, flux penetrates into the cylinders with 60- and 300-nm-thick walls at $H^* = 20$ and 30 Oe, respectively [Fig. 6(a) and inset to upper panel of Fig. 8]. If we assume that H^* is defined by the balance between the positive contribution to the Gibbs energy of the magnetic field in the substrate $F_h = D(H_i - H_0)^2/8\pi$ and the negative condensation energy in the film $F_s = dH_c/8\pi$, then $H^* \propto \sqrt{d/D}$. The thickness of the film in these two samples differs by a factor of five and one could expect for the ratio of H^* $\sqrt{5} \approx 2.2$, while we found 1.5. This shows that the Gibbs energy of the magnetic field in the substrate does not determine the observed value of H^*. This behavior for a superconducting ring was discussed long time ago in Ref. [22]. Such a problem exists also with the critical current of the SSS in bulk samples where the dependence $1/\sqrt{D}$ was not found in experiments. Further experiments and analysis is required to better understand these problems.

B. ac susceptibilities

Measured in constant dc fields, $\chi_1(H_0)$ can be well fitted by our model as the combined response of two SSS, one with $\nu = 0$ in Eq. (11), i.e., with $J_{\rm pin} \to \infty$, and consequently, $\chi_{1p} = -1/4\pi$, and the other with the current independent value of ν. However, this is linear approach and in order to take into account the nonlinear character of the response, the relaxation parameter ν in Eq. (11) has to be current dependent. We assumed that $\nu(J) = \nu_0 J^2$ and try to choose such value of ν_0 that these two SSS provide the presentation of experimental χ_1 data precisely and the best possible approximation of χ_3. In general, Eq. (11) for the first harmonic has no solution for arbitrary χ_1 and given $\nu(J)$. For $H_0 > 0.9H_{c3}$, χ_1 is small and our model did not reproduce the experimental data for these dc fields. For χ_1, the experimental and fitting curves are not distinguishable from each other in a magnetic field lower than $\approx 0.9H_{c3}$ and we did not show the fitting curves in Fig. 9. The fitting curves for $|\chi_3|$ in the frame of the proposed model are shown in Fig. 10. The inset to Fig. 10 shows the field dependence of the parameter p for two amplitudes of excitation. The obtained p's depend on the applied ac amplitude. This is a result of the approximation. Here only two SSS have been considered. Obviously, more SSS with different values of pinning current, $J_{\rm pin}$, should be used. Also, the separation between pinned and unpinned states could depend on the ac amplitude. With increasing ac amplitude, the "effective" part of unpinned states is increasing as expected. We would like to note that the lack of frequency dispersion (Fig. 9) shows that the parameter ν_0 in Eq. (7) is proportional to the frequency. Only in this case the ac response will be frequency independent.

The effect of ramping the dc field on an ac response can be explained as follows. In the absence of any relaxation, i.e., for $\nu(J_s) = 0$ in Eq. (11), the surface current is growing as a function of time $J_s = J_s(0) - \dot{h}_0 t - h_{\rm ac}\sin(\omega t)$, where $J_s(0)$ is the current at the time $t = 0$. At some time, this current exceeds the value of pinning current, $J_{\rm pin}$. In this case, all surface states with different pinning will provide a response that is obviously quite different from the response in a constant dc field. We emulated this effect by the assumption that the driving field in Eq. (11) is $h = \dot{h}_0 t + h_{\rm ac}\sin(\omega T)$ and $\nu(J) = \nu_1(J - J_{\rm pin})$ for $J > J_{\rm pin}$ and $\nu = 0$ otherwise. The results of fitting for χ_1 we do not show in Fig. 11 because experimental and fitting data could not be distinguished. The simulations for $|\chi_2|$ and $|\chi_3|$ are presented in Fig. 12. In contrast to PBP mode, in SF mode, χ_1 depends on the frequency. This is because the dimensionless parameter

$$Q = \frac{\dot{h}_0}{\omega h_{\rm ac}}$$

in Eq. (11) is changed, see also Refs. [13,23]. We have to mention that χ_1 for sets 293 Hz, 0.2 Oe and 1465 Hz, 0.04 Oe, are close to each other, see Fig. 11. The reason for this is that in these two measurements the parameter Q is the same for both sets. This is correct only if ν_1 is proportional to the excitation frequency. An explanation of the experimental results for $H_0 < H_{c2}$ in SF mode can be done in the frame of a model that takes into account vortex motion [4].

VI. CONCLUSION

We have studied the dc and ac magnetic properties of the thin-walled cylinders of superconducting Nb films. dc magnetization curves demonstrate avalanchelike penetration of magnetic flux into the cylinder. The effect was observed at 4.5 K and completely disappeared at 7 K. Such behavior resembles the thermomagnetic instability of vortices but it was observed in fields far below H_{c1} of the film that forms the cylinder walls, i.e., in a vortex-free state. We showed that the thermodynamic criterion is an unlikely description of these magnetization jumps.

The surface superconducting states of a thin-walled cylinder were described. A phenomenological model for the ac response of the surface superconducting state was developed. In this model, it is assumed that the order parameter relaxes to the state with zero current. The proposed model provides a qualitative description of the ac response at the first, second, and third harmonics of the fundamental frequency in point-by-point and swept-field modes.

ACKNOWLEDGMENTS

Fruitful discussions with J. Kolacek and P. Lipavsky are kindly appreciated. We acknowledge a grant from the VEGA agency for financial support for project No. 2/0173/13. We also thank the Unit for Nanocharacterization of Center for Nanoscience and Nanotechnology of the Hebrew University for the SEM images.

[1] W. A. Little and R. D. Parks, Phys. Rev. Lett. **9**, 9 (1962).
[2] D. H. Douglass, Jr., Phys. Rev. **132**, 513 (1963).
[3] K. Aoyama, R. Beaird, D. E. Sheehy, and I. Vekhter, Phys. Rev. Lett. **110**, 177004 (2013).
[4] M. I. Tsindlekht, V. M. Genkin, S. Gazi, and S. Chromik, J. Phys.: Condens. Matter **25**, 085701 (2013).
[5] P. G. de Gennes, *Superconductivity of Metals and Alloys* (Benjamin, New York, 1966), p. 197.
[6] C. Kittel, S. Fahy, and S. G. Louie, Phys. Rev. B **37**, 642(R) (1988).
[7] E. R. Nowak, O. W. Taylor, L. Liu, H. M. Jaeger, and T. I. Selinder, Phys. Rev. B **55**, 11702 (1997).
[8] P. Esquinazi, A. Setzer, D. Fuchs, Y. Kopelevich, E. Zeldov, and C. Assmann, Phys. Rev. B **60**, 12454 (1999); D. Stamopoulos, A. Speliotis, and D. Niarchos, Supercond. Sci. Technol. **17**, 1261 (2004).
[9] D. Saint-James and P. G. Gennes, Phys. Lett. **7**, 306 (1963).
[10] P. Burger, G. Deutscher, E. Gueon, and A. Martinet, Phys. Rev. **137**, A853 (1965).
[11] R. W. Rollins and J. Silcox, Phys. Rev. **155**, 404 (1967).
[12] M. Strongin, D. G. Schweitzer, A. Paskin, and P. P. Craig, Phys. Rev. **136**, A926 (1964).
[13] E. Maxwell and W. P. Robbins, Phys. Lett. **19**, 629 (1966).
[14] M. I. Tsindlekht, V. M. Genkin, G. I. Leviev, Y. Schlussel, V. A. Tulin, and V. A. Berezin, Physica C **473**, 6 (2012).
[15] Y. Schlussel (unpublished).
[16] G. I. Leviev, V. M. Genkin, M. I. Tsindlekht, I. Felner, Yu. B. Paderno, V. B. Filippov, Phys. Rev. B **71**, 064506 (2005).
[17] A. V. Pan and P. Esquinazi, Phys. Rev. B **70**, 184510 (2004).
[18] H. J. Fink and A. G. Presson, Phys. Rev. **151**, 219 (1966).
[19] D. Saint-James, G. Sarma, and E. J. Thomas, *Type II Superconductivity* (Pergamon Press, Oxford, 1969).
[20] H. J. Fink, Phys. Rev. Lett. **14**, 309 (1965); **14**, 853 (1965).
[21] M. I. Tsindlekht, G. I. Leviev, V. M. Genkin, I. Felner, Yu.B. Paderno, and V. B. Filippov, Phys. Rev. B **73**, 104507 (2006).
[22] J. E. Mercereau and T. K. Hunt, Phys. Rev. Lett. **8**, 243 (1962).
[23] H. Fink, Phys. Rev. **161**, 417 (1967).